Role of precursor nuclei in heavy-ion induced reactions at low energies

Ishfaq Majeed Bhat [1,*] Mohd. Shuaib,[1] M. Shariq Asnain,[1] Manoj Kumar Sharma,[2] Abhishek Yadav,[3] Vijay R. Sharma,[4] Pushpendra P. Singh,[5] Devendra P. Singh,[6] Sunita Gupta,[7] Unnati Gupta,[8] Rudra N. Sahoo,[5] Arshiya Sood,[5] Malika Kaushik,[5] Sushil Kumar,[9] R. Kumar,[9] B. P. Singh,[1,†] and R. Prasad[1]

[1]*Nuclear Physics Laboratory, Department of Physics, Aligarh Muslim University, Aligarh 202002, Uttar Pradesh, India*
[2]*Department of Physics, University of Lucknow, Lucknow 226007, Uttar Pradesh, India*
[3]*Department of Physics, Faculty of Natural Sciences, Jamia Milia Islamia, New Delhi 110025, India*
[4]*Istituto Nazionale di Fisica Nucleare, Laboratori Nazionali del Sud, Catania, Italy*
[5]*Department of Physics, Indian Institiute of Technology, Ropar, Punjab 140001, India*
[6]*Department of Physics, University of Petroleum and Energy Studies, Dehradun 248007, India*
[7]*Department of Physics, Agra College, Agra 282002, India*
[8]*Amity Institute of Nuclear Science and Technology, Amity University, Noida-201313, Uttar Pradesh, India*
[9]*Nuclear Physics Group, Inter University Accelerator Center, Aruna Asaf Ali Marg, New Delhi 110067, India*

(Received 24 January 2022; accepted 5 May 2022; published 18 May 2022)

In heavy-ion induced reactions, generally, a large number of residues are populated through different reaction channels. In some cases the same residue is populated via two different modes viz., (i) directly from a given reaction and (ii) via β and/or electron capture decay of a nuclide (precursor). Separation of the two is required for a better understanding of reaction dynamics. The procedure existing in the literature for extracting the independent production cross section from the cumulative cross section employs the assumptions of half-life of the daughter being much larger in comparison to the half-life of the precursor ($t^p_{1/2} \ll t^d_{1/2}$) and require the counting to be performed after large cooling times ($t_l \rightarrow \infty$). A general and more exact expression is obtained in the present work surpassing the assumptions as well as difficulties reported earlier. Analysis of the experimental reaction data sets covering a broader range of possibilities ($t^p_{1/2} > t^d_{1/2}; t^p_{1/2} \approx t^d_{1/2}; t^p_{1/2} < t^d_{1/2}$) presented shows the importance of the current formulations. The advantage of the generalized expression even when the assumptions hold true is also discussed. A comparison of results obtained from the traditional method in the context of its assumptions instead of the calculations from the exact expression has been made. The results obtained with the presently derived formulations are found to give justified values of cross sections for all the cases in contrast to the traditional formulation.

DOI: 10.1103/PhysRevC.105.054607

I. INTRODUCTION

One of the most remarkable growth areas of late in nuclear physics is the study of the interactions of heavy ions (HI's) [1–9]. The HI collisions facilitate the study of a wide range of nuclear interactions—fission, scattering, evaporation-type reactions, stripping reactions, Coulomb excitation, etc. As such, HI reactions are a very rich, fascinating, and rewarding field of investigation, and aptly known as "microcosm of nuclear reaction physics" [10,11]. The development made in the increasingly sophisticated detection equipment for identification and analysis of the many products of these interactions has also played an important role in attracting the researchers to the field. Among the important features of HI collisions, the most important are their semiclassical nature due to short wavelengths and ability to populate nuclear species with very high excitation energies and high spin states as compared to the light ion induced reactions [10]. Nuclear fusion is an important process in heavy-ion reactions. The HI fusion studies were primarily motivated by the search for superheavy or transuranic elements predicted by the nuclear shell model for larger but not established values of Z and N shell closures [12]. HI fusion research nowadays is of paramount importance for understanding many astrophysical processes like the energy production in stars, nucleosynthesis, evolution of massive stars [13,14]. The fusion of two heavy nuclei, in general, populates a nucleus which is proton-rich and lies far away from the line of stability. Such processes are one of the major part of the HI fusion research. As such, the fusion products generally decay towards the bottom of the valley of β stability via β^+ and/or EC decay processes. Fission processes occurring before and after setting in of the equilibrium in the overall nuclear matter of the interacting ions have also been established to occur in HI reactions [15–19]. The fission products are mostly β^- emitters which decay towards the bottom of the valley of β stability, populating several different members of an isobaric series.

Fusion and fission being very dominating processes in HI reactions even at low incident energies, the product nuclei usually do not have appropriate n/p ratio for them to be stable.

*imbhat@myamu.ac.in
†bpsinghamu@gmail.com

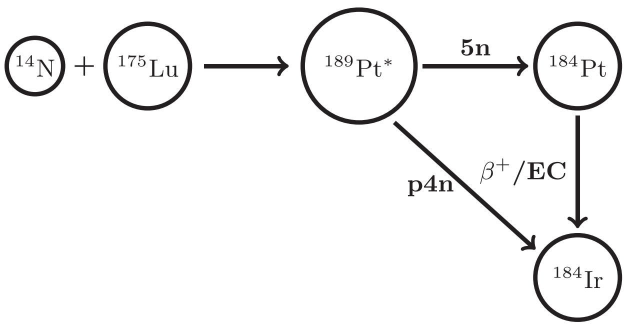

FIG. 1. Direct and the precursor decay contribution in the population of ^{184}Ir.

As a result, the product nuclei often undergo the emission of β-particle and/or electron-capture (EC) decay [20,21]. In β-decay and/or EC processes, the atomic mass number of the nucleus remains the same, but the nuclear charge (atomic number) decreases or increases by one unit. As a result, the nuclei populated independently from the nuclear interactions may also be populated by the β-decay and/or EC process of the precursor nucleus. A representative case of such a process involving the population of ^{184}Ir directly and also through the decay β^+-decay and/or EC process of higher charge precursor ^{184}Pt is shown in Fig. 1. The residues of the type ^{184}Ir have contribution from direct population and also from precursor decay and needs to be separated out. The cross section of the daughter obtained by determining its production rate will be its cumulative cross section. It is desirable to obtain the independent production cross section for the residues from the nuclear reaction only in order to investigate the dynamics of HI reactions accurately so that the predictions of any model calculations may also be verified experimentally.

In literature there exists mathematical formulations of extracting independent activation cross sections from the cumulative ones valid for only specific cases: $t^p_{1/2} \ll t^d_{1/2}$ when the countings have been performed after long cooling time ($t_l \to \infty$), discussed and formulated by Cavinato *et al.* [22]. However, cases with $t^p_{1/2} > t^d_{1/2}$ [23,24] and $t^p_{1/2} \approx t^d_{1/2}$ [25] have been encountered. The difficulties faced in and subsequently giving up altogether on extracting the independent cross section with $t^p_{1/2} \approx t^d_{1/2}$ by Giri *et al.* [25] is a good case in point.

In the present work, the precursor feeding is confronted in a general way eliminating the assumptions [22] and difficulties reported earlier [25,26]. Three systems involving the precursor decay feeding have been considered in the present study: ^{175}Lu(^{14}N, $p4n$) ^{184}Ir ($t^d_{1/2} = 3.09$ h) with precursor feeding from ^{175}Lu(^{14}N, $5n$) ^{184}Pt ($t^p_{1/2} = 17.3$ min) and ^{167}Yb ($t^d_{1/2} = 17.5$ min) with precursor feeding from ^{167}Lu ($t^p_{1/2} = 51.5$ min) in two systems ^{12,13}C + ^{159}Tb [23,24]. All three systems were studied for two different incident energies for consistency. Brief experimental details and data analysis are presented in Sec. II while the cumulative count rate decay curves obtained for all the studied reactions along with their interpretations are given in Sec. III. A general mathematical formulation for deducing the independent production cross section of the daughter nuclei from the cumulative cross section is presented in the Appendix. Results and discussion regarding the application of the generalized formulation are given in Sec. IV. The present work is summarized in Sec. V.

II. EXPERIMENTAL PROCEDURE TO DETERMINE PRODUCTION CROSS SECTION OF REACTION RESIDUES

The experiments for the measurement of excitation functions (EF's) were carried out using ^{14}N beam from Pelletron accelerator facility at the Inter University Accelerator, New Delhi, India. The ion beam is made incident normally on a stack of alternate target and catcher (Al) foils of thickness $\approx$1.2–2.1 mg/cm^2 and 1.5–2.5 mg/cm^2, respectively. The Al foils in the stack serve the two-fold purpose of energy degradation of the beam and stopping in them the energetic recoiling residual nuclei produced during the interaction. The stacked foil activation technique [27] has been used to cover a broad energy range for the EF measurements. The energy degradation in the target and Al foils makes possible multiple energy incidences in single irradiation. The resulting incident energy on each foil of the stack was estimated using the stopping power code SRIM [28]. The irradiations were carried out in the general purpose scattering chamber (GPSC) having an in-vacuum transfer (ITF) facility for quick transfer of the irradiated samples to the γ-ray detection system. The stacks were bombarded for $\approx$8–10 hours each, considering the irradiation times required for the optimum yield of most of the desired channels (residues) at the end of the irradiation. The beam current is monitored using a Faraday cup installed downstream the beam-line behind the target catcher foil assembly, and the beam current was maintained $\approx$4 pnA during the irradiations. The activities induced in the irradiated samples were recorded using a precalibrated ORTEC HPGe detector coupled to a CAMAC based data acquisition system CANDLE [29]. Standard γ sources of ^{60}Co, ^{133}Ba, and ^{152}Eu of known strengths were used for the energy calibration. Absolute photopeak efficiency of the spectrometer for a wide energy range at different source-detector separations were determined before the γ-ray spectroscopic analysis of the irradiated samples was carried out with it. A typical γ spectrum obtained for the ^{14}N + ^{175}Lu system for $E_{\rm lab} = 87.11 \pm 0.89$ MeV is shown in Fig. 2. The γ peaks corresponding to the characteristic γ lines of ^{184}Ir($p4n$) ($E_\gamma = 263.95$ and 390.37 keV), ^{184}Pt($5n$) ($E_\gamma = 154.90$ and 191.97 keV) and the annihilation peak ($E_\gamma = 511$ keV) are marked in the spectrum. The reaction residues ^{184}Ir with precursor feeding from β^+ and/or EC decay of ^{184}Pt residues populated in the same irradiation via the reaction ^{175}Lu(^{14}N, $5n$) has been analyzed at two beam energies ($E_{\rm lab}$) of 87.11 $\pm$ 0.89 MeV and 79.68 $\pm$ 0.96 MeV. The half-life of the precursor ^{184}Pt is 17.3 min while that of the daughter ^{184}Ir is 3.09 h. The reactions $^{159}Tb(^{12}C, p3n)^{167}Yb$ [23] and $^{159}Tb(^{13}C, p4n)^{167}Yb$ [24] were studied at $E_{\rm lab} = 77.77 \pm 0.62$ MeV, 69.15 $\pm$ 0.85 MeV and 84.59 $\pm$ 0.53 MeV, 77.87 $\pm$ 0.61 MeV, respectively. In these cases, ^{167}Lu (populated via $4n$- and $5n$-reaction channels in ^{12}C + ^{159}Tb and ^{13}C + ^{159}Tb systems, respectively) with half-life equal to 51.5 min acts as the precursor which

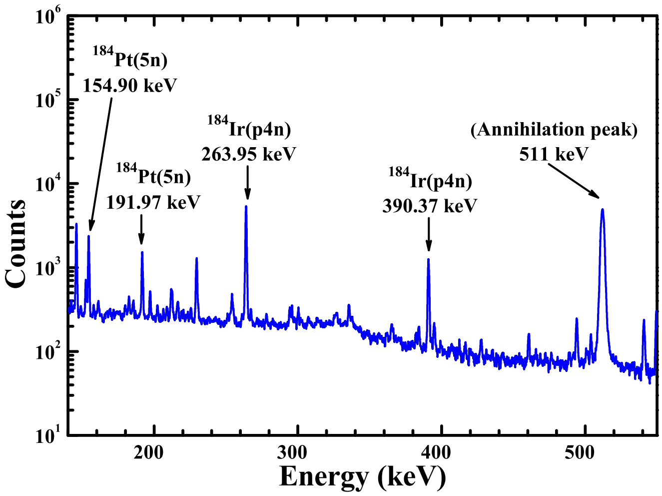

FIG. 2. A typical γ-ray spectrum of the irradiated sample for $^{14}N + ^{175}Lu$ system at $E_{lab} = 87.11 \pm 0.89$ MeV. (See text for more details.)

undergoes EC/β^+ decay populating ^{167}Yb residues with the half-life of 17.5 min.

A. Formulation

In a typical binary nuclear reaction an energetic beam of incident particles 'a', hit a thin foil of target particles 'X', producing a residual nucleus 'Y', and emitting lighter particles of type 'b'. Such a reaction may be represented as $a + X \rightarrow Y + b$. The most sought after observable in nuclear reactions is the cross section which, in general, is a measure of the probability for a particular reaction channel, say r, to occur [30]. In a typical experiment, the rates of production of different nuclides in the final state are counted. Such rates, in general, are proportional [31] to the number (initial) of nuclei N_X in the target-foil illuminated by the beam, and the the flux (J) of the incident beam. Thus, the rate R at which particular nuclides may be produced is $R = \sigma J N_X$, where σ is the constant of proportionality and is the reaction cross section for the reaction which results in the production of such nuclide. If the nuclides are radioactive, the reaction rate R may be easily determined in terms of its directly observable characteristic, i.e., the induced activity. The cross section for the population of the nuclide, thus, measured is referred to as the activation production cross section [32,33]. The number of the populated nuclides goes on increasing owing to its production at the rate R and also decreases due to its own decay. The change in the number of nuclei of interest may be given as

$$dN = Rdt - \lambda N dt, \quad (1)$$

where λ is the decay constant. Solving this gives, for $t \leqslant t_i$,

$$N(t) = \frac{R}{\lambda}[1 - \exp(-\lambda t)], \quad (2)$$

where t_i is the irradiation time. For $t \geqslant t_i$, the radioactive nuclei will decay following the simple exponential decay with initial number being $N(t_i)$ given by Eq. (2). Therefore, for $t \geqslant t_i$,

$$N = \frac{R}{\lambda}[1 - \exp(-\lambda t_i)] \exp(-\lambda t_l),$$

where t_l is the cooling time (time elapsed since the stop of the irradiation). As such, the cross section may be represented by

$$\Rightarrow \sigma = \frac{A \exp(\lambda t_l)}{[1 - \exp(-\lambda t_i)] J N_X}, \quad (3)$$

where A is the activity (decay rate) of the radioactive nuclei. More complex scenarios than the simplest one considered above can arise in activation analysis [32,34]. It is quite likely that particular nuclides may be produced directly from the primary experimental reaction and the same nuclides are populated via the decay of another nuclide produced in the same experiment. As already mentioned, the most common example of the situation, which is particularly important in the present work, is feeding of a reaction residue by its higher charge precursor isobars via an electron capture [20] process and/or β^+ decay [21]. The deduction of the independent cross section from the cumulative cross sections for such a case may be carried out by solving general Bateman equations [35]. As already mentioned, the formulation provided by Cavinato *et al.* [22] is valid under the stringent assumption of $t^p_{1/2} \ll t^d_{1/2}$ and the calculations are to be performed with countings performed after a substantially long time when the precursor has assumed to be completely decayed to the daughter nuclei. The mathematical procedure to determine the independent cross sections in different scenarios ($t^p_{1/2} > t^d_{1/2}$, $t^p_{1/2} \approx t^d_{1/2}$, and $t^p_{1/2} < t^d_{1/2}$) is derived without any simplifying assumptions. The general expression obtained (see the Appendix) connecting the cumulative cross section (σ^c_d), independent production cross section of daughter (σ_d), and the precursor cross section σ_p is

$$\sigma_d{}^c(t_l) = \left[\sigma_d + \frac{P_p \lambda_p}{(\lambda_p - \lambda_d)}\sigma_p\right] - \frac{P_p \lambda_d \sigma_p \exp((\lambda_d - \lambda_p)t_l)}{(\lambda_p - \lambda_d)} \frac{[1 - \exp(-\lambda_p t_i)]}{[1 - \exp(-\lambda_d t_i)]}. \quad (4)$$

As can be seen from Eq. (4) that it connects the cumulative and the independent production cross section of the daughter nuclei and the cross section of the parent corresponding to different lapse times. It turns out that independent cross sections are independent of irradiation time and cooling times.

III. DATA ANALYSIS

The representative cumulative decay curves for $^{184}Ir(p4n)$ with precursor decay feeding from $^{184}Pt(5n)$ populated in the $^{14}N + ^{175}Lu$ system at $E_{lab} = 87.11 \pm 0.89$ MeV and 79.68 ± 0.96 MeV obtained for its characteristic γ ray 263.95 keV [36] are shown in Fig. 3(a) and (b), respectively. Since $t^p_{1/2} < t^d_{1/2}$ in this case, the precursor ^{184}Pt quickly decays and the daughter ^{184}Ir count rates rise to a maximum and then decays with its characteristic half-life. An attempt has been made to verify this by fitting the last cumulative count rates with a

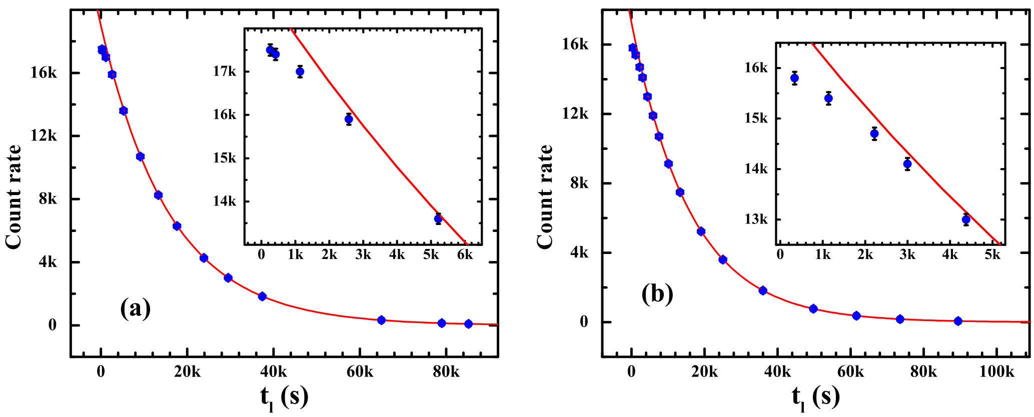

FIG. 3. Cumulative count rate decay curves for $^{184}Ir(p4n)$ residues with precursor decay feeding from $^{184}Pt(5n)$ populated in $^{14}N + {}^{175}Lu$ for (a) $E_{\text{lab}} = 87.11 \pm 0.89$ MeV and (b) $E_{\text{lab}} = 79.68 \pm 0.96$ MeV. The red curves represent the exponential decay fit to the last three count rates. (See text for more details.)

simple exponential decay function of the form

$$f(t) = ae^{-bt}, \tag{5}$$

where a and b are the fitting parameters. Also, because the minimum number of data points required to fit the two parameter model (ae^{-bt}) is three, the fitting has been done with the last three cumulative count rates in Fig. 3. The fitted curves are shown in red color. The fact that the precursor nuclei (^{184}Pt) quickly decay and the daughter nuclei (^{184}Ir) then decay with its characteristic half-life can be readily observed from the decay curves. The curves fitted to the last three count rates agrees well with the count rates corresponding to the earlier count rates also. However, as expected, the count rates for very small t_l values fall below the fitted curve as is evident from the smaller lapse times shown in the zoomed-in decay curves shown in the inset graphs. Comparing Eq. (5) with the standard radioactive exponential decay function $A_0e^{-\lambda t}$, the half-life for the last count rates is

$$t_{1/2}^{p} = \frac{\ln(2)}{b}. \tag{6}$$

The values of $t_{1/2}$ obtained in this manner along with the fitting errors are given in Table I. The half-life obtained via Eq. (6) for both the incident energies (given in Table I) agrees well with the literature value of ^{184}Ir half-life (3.09 h).

The residues ^{167}Yb are populated directly via the reaction $^{159}Tb(^{12}C, p3n)$ and $^{159}Tb(^{13}C, p4n)$ and also by the decay of precursor ^{167}Lu produced via $^{159}Tb(^{12}C, 4n)$ and $^{159}Tb(^{13}C, 5n)$ reactions, respectively. The decay curves corresponding to ^{167}Yb residues from $^{159}Tb(^{12}C, p3n)$ [23] and $^{159}Tb(^{13}C, p4n)$ reactions for $E_\gamma = 176.23$ keV are shown in Figs. 4 and 5, respectively. Since the half-life of the precursor ^{167}Lu ($t_{1/2}^{p} = 51.5$ min) in this case is almost three times the half-life of the daughter ^{167}Yb ($t_{1/2}^{p} = 17.5$ min), the daughter nuclei decays with the half-life of the precursor for large lapse times under the transient equilibrium [30] condition. An attempt has been made to verify the setting in of the transient equilibrium condition by fitting the last cumulative count rates (as discussed earlier) for all the cases [Figs. 4(a)–5(b)]. The fitted curves are shown in red color in the cumulative count rate decay curves. The values of $t_{1/2}$ obtained in this manner along with the fitting errors are given in Table I. As can be seen from this table, the half-life of the precursor nuclei ^{167}Yb obtained in all the cases is in agreement with the half-life value in literature. The smaller t_l portions of the zoomed-in decay curves have been shown in the inset graphs to highlight the fact that the transient equilibrium is set in for large t_l values only and the count rates for the counting performed at smaller t_l fall below the fitted red curve and do not vary in accordance with the characteristic exponential decay curve. This behavior of the early count rates shows the time during which the daughter nuclei (^{167}Yb) are being populated from the precursor (^{167}Lu) decay besides their radioactive decay.

IV. RESULTS AND DISCUSSION

Intensity of the γ line of the parent nuclide have been used to determine the cross section of the precursor, i.e., σ_p. On

TABLE I. Half-lives obtained from the last cumulative count rate decay curves of the daughter nuclei fed by the precursor nuclei. (See text for more details.)

System	Energy (MeV)	Residue	Measured $t_{1/2}$	Literature $t_{1/2}$	Shown in
$^{14}N + {}^{175}Lu$	87.11 ± 0.89	^{184}Ir	3.09 ± 0.01 h	3.09 h	Fig. 3(a)
	79.68 ± 0.96	^{184}Ir	3.08 ± 0.03 h	3.09 h	Fig. 3(b)
$^{12}C + {}^{159}Tb$	77.77 ± 0.62	^{167}Lu	51.66 ± 0.28 min	51.5 m	Fig. 4(a)
	69.15 ± 0.85	^{167}Lu	51.18 ± 0.43 min	51.5 min	Fig. 4(b)
$^{13}C + {}^{159}Tb$	84.59 ± 0.53	^{167}Lu	51.19 ± 0.24 min	51.5 min	Fig. 5(a)
	77.87 ± 0.61	^{167}Lu	51.54 ± 0.15 min	51.5 min	Fig. 5(b)

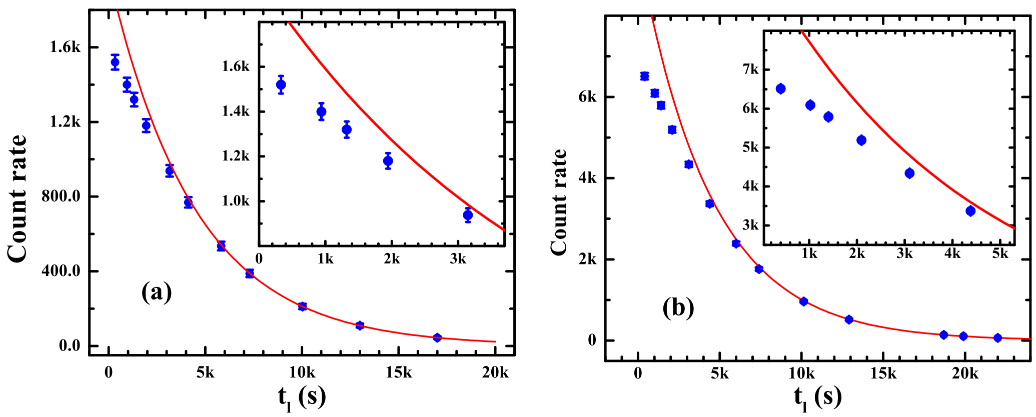

FIG. 4. Cumulative count rate decay curves for $^{167}Yb(p3n)$ residues with precursor decay feeding from $^{167}Lu(4n)$ populated in $^{12}C + {}^{159}Tb$ for (a) $E_{\rm lab} = 77.77 \pm 0.62$ MeV and (b) $E_{\rm lab} = 69.15 \pm 0.85$ MeV. The red curves represent the exponential decay fit to the last three count rates. (See text for more details.)

the other hand, the intensity of the γ line of the daughter nuclei cumulative production cross section σ_c^d was obtained and was employed to deduce the independent production cross section of the daughter nuclides σ_d. It has been observed that it gives the independent cross section of the daughter residues (σ_d) regardless of the cooling time (t_l) and the value of λ_d/λ_p. This equation can also be used for extracting the independent cross section of daughter under the situations when $t_{1/2}^p \approx t_{1/2}^d$ (problem faced in Ref. [25]).

Taking limits as $t_l \to \infty$ and $\lambda_d/\lambda_p \to 0$, the limiting value of the third (unbracketed) term in Eq. (4) becomes

$$\begin{aligned}
&\lim_{\lambda_d/\lambda_p\to 0}\lim_{t_l\to\infty} \frac{P_p\lambda_d\sigma_p \exp((\lambda_d-\lambda_p)t_l)}{(\lambda_p-\lambda_d)}\frac{[1-\exp(-\lambda_p t_i)]}{[1-\exp(-\lambda_d t_i)]}\\
&= P_p\sigma_p\frac{[1-\exp(-\lambda_p t_i)]}{[1-\exp(-\lambda_d t_i)]}\lim_{\lambda_d/\lambda_p\to 0}\lim_{t_l\to\infty}\frac{\lambda_d}{(\lambda_p-\lambda_d)}[\exp((\lambda_d-\lambda_p)t_l)]\\
&= P_p\sigma_p\frac{[1-\exp(-\lambda_p t_i)]}{[1-\exp(-\lambda_d t_i)]}\lim_{\lambda_d/\lambda_p\to 0}\lim_{t_l\to\infty}\frac{\lambda_d}{\lambda_p}\left(1-\frac{\lambda_d}{\lambda_p}\right)^{-1}\left[\exp\left(-\left(1-\frac{\lambda_d}{\lambda_p}\right)\lambda_p t_l\right)\right]\\
&= P_p\sigma_p\frac{[1-\exp(-\lambda_p t_i)]}{[1-\exp(-\lambda_d t_i)]}\lim_{\lambda_d/\lambda_p\to 0}\lim_{t_l\to\infty}\frac{\lambda_d}{\lambda_p}\left(1-\frac{\lambda_d}{\lambda_p}\right)^{-1}\frac{1}{\left[\exp\left(\left(1-\frac{\lambda_d}{\lambda_p}\right)\lambda_p t_l\right)\right]} = 0. \qquad (7)
\end{aligned}$$

It may be noted that the factors to the left of the limits in second step are all equal to finite nonzero numbers independent of the values of λ_d and λ_p. Thus, Eq. (4) under the given limits reduces to

$$\lim_{\lambda_d/\lambda_p\to 0}\lim_{t_l\to\infty}\sigma_d{}^c = \sigma_d + \frac{P_p\lambda_p}{\lambda_p-\lambda_d}\sigma_p. \qquad (8)$$

This is the simplified equation given by Cavinato *et al.* [22] and if applied for all the cases ($\lambda_p > \lambda_d$ and $\lambda_p < \lambda_d$) may lead to erroneous results. For practical purposes, also, the limit of $t_l \to \infty$ may be not be realistic as it may require counting runs at extremely long times after irradiation unless the half-life of the daughter nuclide is relatively small [26]. The other limit $\lambda_d/\lambda_p \to 0$ is also a relative assumption and may vary according the precision and accuracy of the measurement required. This assumption also ignores entirely the other regime of possibilities $t_{1/2}^p > t_{1/2}^d$ [23,24] and $t_{1/2}^p \approx t_{1/2}^d$ [25]. Thus, Eq. (4) derived in the present work is more general that can be used in all possible cases unlike Eq. (8). A close observation of Eq. (8) also suggests the possibility of obtaining negative values of σ_d which is not realistic. The independent cross sections of the daughter nuclides obtained via the calculations performed using the more generalized Eq. (4) ($\sigma_{\rm ind}^{\rm exact}$ from now on) are shown in Fig. 6(a) for $^{184}Ir(p4n)$ in $^{14}N + {}^{175}Lu$ corresponding to $E_{\rm lab} = 87.11 \pm 0.89$ MeV. The cross sections calculated as such turn out to be independent of lapse time. The cross sections shown in Fig. 6(a) deduced at different times are found to be consistent within experimental uncertainties as well. The dashed blue line shows the weighted average of independent cross section of $\sigma_{\rm ind}^{\rm exact}$ values for the different counting runs ($\overline{\sigma_{\rm ind}^{\rm exact}}$). The red solid line shown in Fig. 6(a) corresponds to the theoretically predicted value of the cross section ($\sigma_{\rm theoretical}$ from now on) for the reaction $^{175}Lu(^{14}N, p4n)^{184}Ir$ at $E_{\rm lab} = 87.11 \pm 0.89$ MeV. The theoretical value has been taken from the model code PACE4 [37], a statistical Monte Carlo code for evaporation residue population from the compound nucleus decay

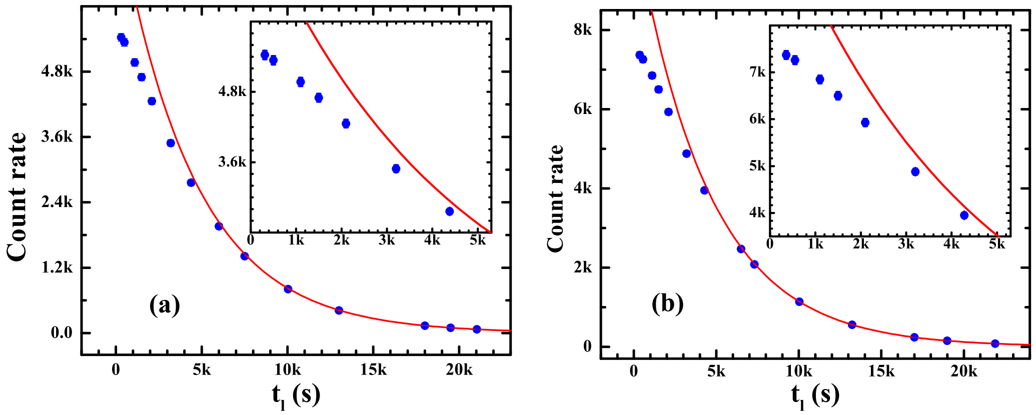

FIG. 5. (a) Cumulative count rate decay curves for $^{167}Yb(p4n)$ residues with precursor decay feeding from $^{167}Lu(5n)$ populated in $^{13}C + ^{159}Tb$ for (a) $E_{\text{lab}} = 84.59 \pm 0.53$ MeV and (b) $E_{\text{lab}} = 77.87 \pm 0.61$ MeV. The red curves represent the exponential decay fit to the last three count rates. (See text for more details.)

employing the parameters which reproduce the excitation functions of other CF channels as well. PACE4 uses the Hauser-Feshbach formalism [38]. It involves an effective procedure to couple angular momentum at each stage of de-excitation of the excited compound nuclei that facilitates monitoring the angular distribution of evaporated particles at each stage of de-excitation. The transmission coefficients for light nuclear particles like n, p, and α emissions are calculated using the optical model potential [39] whereas the Bass model [40] is used to determine the fusion cross section. The excitation energy-dependent level density parameter from Kataria *et al.* [41] and Gilbert and Cameron [42] are used. The level density is obtained using $a = A/K$, where A is the compound nucleus mass number, and K is a free parameter. K is generally varied with values of 8, 9, and 10 to check the variation of the residual cross section with respect to K. The agreement between the experimentally measured and theoretically predicted value of the cross section validates the experimental methodology presented for the determination of the independent cross section of the daughter nuclides. On the other hand, Fig. 6(b) shows the independent cross sections obtained via the traditional method [22] given in Eq. (8) ($\sigma_{\text{ind}}^{\text{trad}}$ from now on) from the different counting runs of the daughter $^{184}Ir(p4n)$. As can be seen from this figure, the independent cross sections are found to be time dependent. Also, as mentioned earlier, the cross sections calculated using the traditional method [22] turn out to be negative (unrealistic) for smaller lapse times. For the longer lapse times with $t_{1/2}^{d} \gg t_{1/2}^{p}$, however, the cross sections tend to be equal to the expected value in line with the result of Eq. (8). Similar arguments hold for this reaction [$^{175}Lu(^{14}N, p4n)^{184}Ir$] at $E_{\text{lab}} = 79.68 \pm 0.96$ MeV and are represented in Fig. 7.

The independent cross sections $\sigma_{\text{ind}}^{\text{exact}}$ deduced from Eq. (4), derived in the present work, of $^{167}Yb(p3n)$ residues in $^{12}C + ^{159}Tb$ corresponding to $E_{\text{lab}} = 77.77 \pm 0.62$ MeV are shown in Fig. 8(a) for the different countings run. Similar to the first case, the values of $\sigma_{\text{ind}}^{\text{exact}}$ are also found to be time independent within experimental uncertainties. The dashed blue

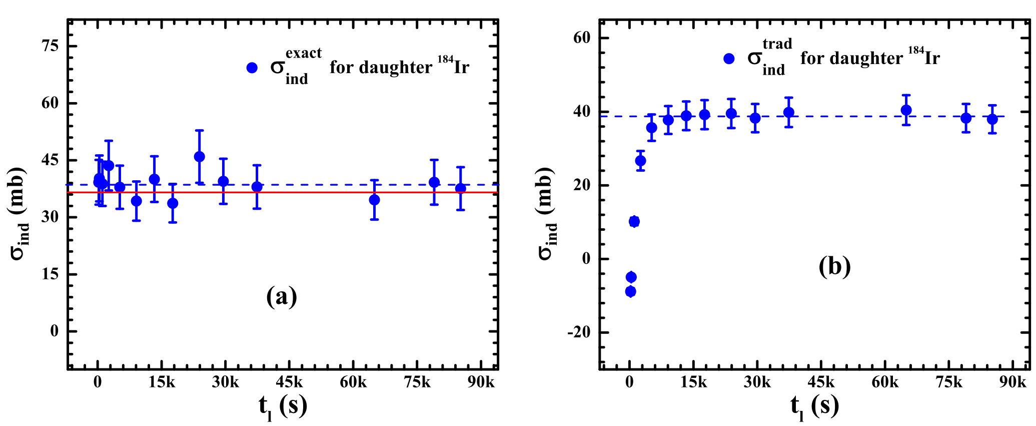

FIG. 6. (a) Primary irradiation independent production cross sections $\sigma_{\text{ind}}^{\text{exact}}$ of the daughter $^{184}Ir(p4n)$ in $^{14}N + ^{175}Lu$ at $E_{\text{lab}} = 87.11 \pm 0.89$ MeV for different counting runs corresponding to different lapse times. The dashed blue line corresponds to the weighted average independent cross section of $\sigma_{\text{ind}}^{\text{exact}}$ values for the different counting runs ($\overline{\sigma_{\text{ind}}^{\text{exact}}}$). The solid red line represents the theoretically predicted value of cross-section for the considered reaction at this energy. (b) Primary irradiation independent production cross sections $\sigma_{\text{ind}}^{\text{trad}}$ of the daughter ^{184}Ir for counting runs at different lapse times.

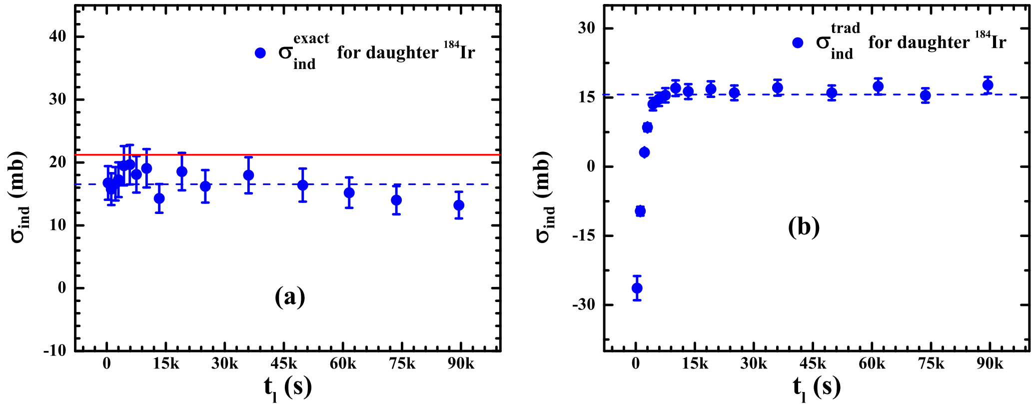

FIG. 7. (a) Primary irradiation independent production cross sections $\sigma_{\rm ind}^{\rm exact}$ of the daughter $^{184}Ir(p4n)$ in $^{14}N + {}^{175}Lu$ at $E_{\rm lab} = 79.68 \pm 0.96$ MeV for different counting runs corresponding to different lapse times. The dashed blue line corresponds to $\overline{\sigma_{\rm ind}^{\rm exact}}$. The solid red line represents the theoretically predicted value of cross section for the considered reaction at this energy. (b) Primary irradiation independent production cross sections $\sigma_{\rm ind}^{\rm trad}$ of the daughter ^{184}Ir for counting runs at different lapse times.

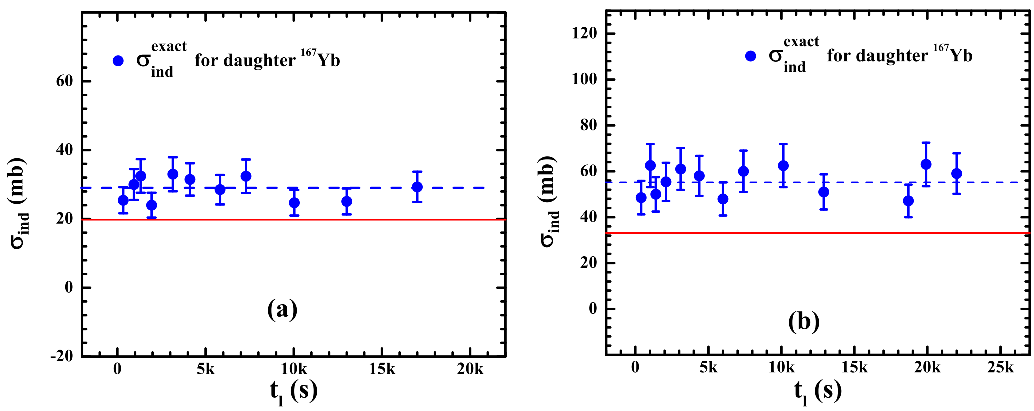

FIG. 8. Primary irradiation independent production cross sections $\sigma_{\rm ind}^{\rm exact}$ of the daughter $^{167}Yb(p3n)$ in $^{12}C + {}^{159}Tb$ for different counting runs corresponding to different lapse times. The dashed blue line corresponds to $\overline{\sigma_{\rm ind}^{\rm exact}}$. The solid red line represents the theoretically predicted value of cross section for the considered reaction at the respective energies (see text for more details). (a) $E_{\rm lab} = 77.77 \pm 0.62$ MeV, (b) $E_{\rm lab} = 69.15 \pm 0.85$ MeV.

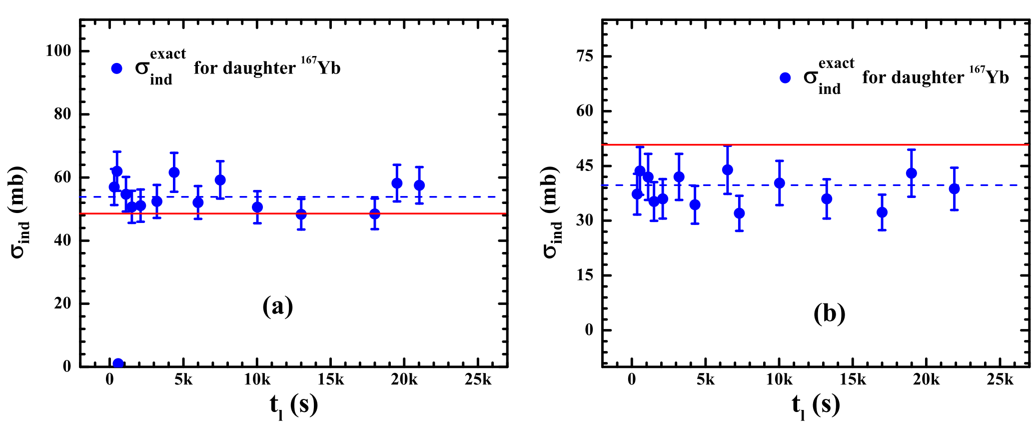

FIG. 9. (a) Primary irradiation independent production cross sections $\sigma_{\rm ind}^{\rm exact}$ of the daughter $^{167}Yb(p4n)$ in $^{13}C + {}^{159}Tb$ for different counting runs corresponding to different lapse times. The dashed blue line corresponds to $\overline{\sigma_{\rm ind}^{\rm exact}}$. The solid red line represents the theoretically predicted value of the cross section for the considered reaction at the respective energies (see text for more details). (a) $E_{\rm lab} = 84.59 \pm 0.53$ MeV, (b)$E_{\rm lab} = 77.87 \pm 0.61$ MeV.

TABLE II. Weighted average of the deduced independent cross sections and the corresponding theoretical predictions.

System	Reaction	Energy (MeV)	$\overline{\sigma_{\rm ind}^{\rm exact}}$ (mb)	$\sigma_{\rm theoretical}$ (mb)
$^{14}N + ^{175}Lu$	$^{175}Lu(^{14}N, p4n)^{184}Ir$	87.11 ± 0.89	38.89 ± 5.82	36.50
		79.68 ± 0.96	16.58 ± 2.68	21.2
$^{12}C + ^{159}Tb$	$^{159}Tb(^{12}C, p3n)^{167}Yb$	77.77 ± 0.62	29.01 ± 4.71	19.7
		69.15 ± 0.85	55.34 ± 8.38	33.10
$^{13}C + ^{159}Tb$	$^{159}Tb(^{13}C, p4n)^{167}Yb$	84.59 ± 0.53	53.86 ± 5.45	48.40
		77.87 ± 0.61	39.68 ± 5.75	50.80

and solid red lines represent similar quantities as in Fig. 6. The values of the experimentally measured cross sections from the countings performed at different cooling times lie close to the theoretical cross section. This vindicates the generalized expression Eq. (4) and procedure of obtaining the independent production cross section of the daughter nuclide with precursor feeding. Similar arguments hold for $^{167}Yb(p3n)$ in $^{12}C + ^{159}Tb$ corresponding to $E_{\rm lab} = 69.15 \pm 0.85$ MeV and are represented in Fig. 8(b). The parent and daughter residues being same in $^{13}C + ^{159}Tb$ also show similar behavior at both the studied energies of $E_{\rm lab} = 84.59 \pm 0.53$ MeV and $E_{\rm lab} = 77.87 \pm 0.61$ MeV and are shown in Fig. 9(a) and (b), respectively. The experimentally deduced cross sections using the generalized approach and the theoretical predictions for the HI systems and energies considered are given in Table II.

As such, the derived Eq. (4) is a general way out to separate precursor contributions in the daughter nuclei decays to yield its independent production cross sections in a nuclear reaction experiment.

V. CONCLUSIONS

In the present work a general expression for separating out the independent production cross section of the reaction residues having feeding from precursor decay has been obtained. The expression obtained has been found to give better results in all the conditions of relative half-lives of precursor and daughter nuclei. The anomalies in the results obtained from the traditional method/expression have also been overcome in the present work. The general expression presented in the work yields the correct and lapse-time independent cross section values and eliminates the requirement of counting to be performed after long cooling times. The results obtained with the new procedure will be useful for better and useful predictions of the theoretical models.

ACKNOWLEDGMENTS

Thanks are due to the Chairperson, Department of Physics A. M. U., Aligarh for providing all the necessary facilities to carry out this work. The authors (B.P.S. and M.S.A.) also thank the DST-SERB Project No. CRG/2020/000136 for financial support. The authors also thank the Director of IUAC, New Delhi, India and the staff of the target laboratory IUAC for helping in the fabrication of samples/targets. Besides, all authors thank IIT Ropar, India for providing HPGe detector for the experiments.

APPENDIX: MATHEMATICAL STRUCTURE FOR PRECURSOR DECAY FEEDING

Suppose a radioactive nuclide, say d is populated directly from the reaction $a + X$ and by decay of any other nucleus, say p (known as precursor for d) also formed in the reaction with a branching ratio equal to P_p. Therefore, for $t \leqslant t_i$ as quoted by Cavinato *et al.* [22],

$$\frac{dN_p}{dt} = JN_X\sigma_p - \lambda_p N_p \tag{A1}$$

and

$$\frac{dN_d}{dt} = JN_X\sigma_d - \lambda_d N_d + P_p\lambda_p N_p. \tag{A2}$$

For $t > t_i$, we have

$$\frac{dN_p}{dt} = -\lambda_p N_p \tag{A3}$$

$$\Rightarrow N_p = N_p(t_i)\exp(-\lambda_p t_l)$$
$$\Rightarrow N_p = \frac{JN_X\sigma_p}{\lambda_p}[1 - \exp(-\lambda_p t_i)]\exp(-\lambda_p t_l) \tag{A4}$$

and

$$\frac{dN_d}{dt} = -\lambda_d N_d + P_p\lambda_p N_p. \tag{A5}$$

Equations (A1) and (A2) are coupled differential equations and so are Eqs. (A3) and (A5). Multiplying Eqs. (A1) and (A3) by $\frac{P_p\lambda_p}{(\lambda_p - \lambda_d)}$ and their respective addition to Eqs. (A2) and (A5) yields for $t \leqslant t_i$,

$$\frac{d}{dt}\left(N_d + \frac{P_p\lambda_p}{\lambda_p - \lambda_d}N_p\right) = \left(\sigma_d + \frac{P_p\lambda_p}{\lambda_p - \lambda_d}\sigma_p\right)JN_X - \lambda_d\left(N_d + \frac{P_p\lambda_p}{\lambda_p - \lambda_d}N_p\right)$$
$$\Rightarrow \frac{d}{dt}\left(N_d + \frac{P_p\lambda_p}{\lambda_p - \lambda_d}N_p\right) + \lambda_d\left(N_d + \frac{P_p\lambda_p}{\lambda_p - \lambda_d}N_p\right) = \left(\sigma_d + \frac{P_p\lambda_p}{\lambda_p - \lambda_d}\sigma_p\right)JN_X \tag{A6}$$

and for $t \geqslant t_i$, we get

$$\frac{d}{dt}\left(N_d + \frac{P_p\lambda_p}{\lambda_p - \lambda_d}N_p\right) = -\lambda_d\left(N_d + \frac{P_p\lambda_p}{\lambda_p - \lambda_d}N_p\right). \tag{A7}$$

Equation (A6) being a linear differential equation of first order in $(N_d + \frac{P_p\lambda_p}{\lambda_p-\lambda_d}N_p)$ gives its solution as for $t \leqslant t_i$,

$$\left(N_d + \frac{P_p\lambda_p}{\lambda_p - \lambda_d}N_p\right)\exp(\lambda_d t) = \int\left[\left(\sigma_d + \frac{P_p\lambda_p}{\lambda_p - \lambda_d}\sigma_p\right)\right]JN_X\exp(\lambda_d t)dt + C.$$

Assuming N_X and J as constants [30], the above expression yields

$$\left(N_d + \frac{P_p\lambda_p}{\lambda_p - \lambda_d}N_p\right)\exp(\lambda_d t) = \left(\sigma_d + \frac{P_p\lambda_p}{\lambda_p - \lambda_d}\sigma_p\right)JN_X\int\exp(\lambda_d t)dt + C$$

$$\Rightarrow \left(N_d + \frac{P_p\lambda_p}{\lambda_p - \lambda_d}N_p\right)\exp(\lambda_d t) = \frac{1}{\lambda_d}\left[\left(\sigma_d + \frac{P_p\lambda_p}{\lambda_p - \lambda_d}\sigma_p\right)\right]JN_X\exp(\lambda_d t) + C.$$

With initial conditions of $N_p = N_d = 0$ at $t = 0$, the above equation becomes

$$\left[N_d + \frac{P_p\lambda_p}{\lambda_p - \lambda_d}N_p\right]_{(t=t_i)} = \frac{1}{\lambda_d}\left[\left(\sigma_d + \frac{P_p\lambda_p}{\lambda_p - \lambda_d}\sigma_p\right)\right]JN_X[1 - \exp(-\lambda_d t_i)]. \tag{A8}$$

Solving Eq. (A7) gives, for $t > t_i$,

$$N_d + \frac{P_p\lambda_p}{\lambda_p - \lambda_d}N_p = \left[N_d + \frac{P_p\lambda_p}{\lambda_p - \lambda_d}N_p\right]_{t_i} \times \exp(-\lambda_d t_l).$$

Using Eq. (A8) above, we get

$$N_d = \frac{1}{\lambda_d}\left[\left(\sigma_d + \frac{P_p\lambda_p}{\lambda_p - \lambda_d}\sigma_p\right)\right]JN_X[1 - \exp(-\lambda_d t_i)]\exp(-\lambda_d t_l) - \frac{P_p\lambda_p}{\lambda_p - \lambda_d}N_p.$$

Using Eq. (A4), we get, for $t > t_i$,

$$N_d = \frac{1}{\lambda_d}\left[\left(\sigma_d + \frac{P_p\lambda_p}{\lambda_p - \lambda_d}\sigma_p\right)\right]JN_X[1 - \exp(-\lambda_d t_i)]\exp(-\lambda_d t_l) - \frac{P_p}{\lambda_p - \lambda_d}JN_X\sigma_p[1 - \exp(-\lambda_p t_i)]\exp(-\lambda_p t_l).$$

Rearranging and using the terminology defined in the Introduction, we get

$$\frac{A_d\exp(\lambda_d t_l)}{[1 - \exp(-\lambda_d t_i)]JN_X} = \left[\sigma_d + \frac{P_p\lambda_p}{\lambda_p - \lambda_d}\sigma_p\right] - \frac{P_p\lambda_d\sigma_p}{\lambda_p - \lambda_d}[\exp((\lambda_d - \lambda_p)t_l)]\frac{[1 - \exp(-\lambda_p t_i)]}{[1 - \exp(-\lambda_d t_i)]}. \tag{A9}$$

The left-hand side (lhs) of the above equation is in the form of the cross section as can be observed in comparison with Eq. (3). As A_d gives the cumulative decay rate of the daughter nuclei, the lhs gives the cumulative cross section of daughter at the lapse time $= t_l$ (i.e., ${\sigma_d}^c$). Thus, above equation reduces to

$${\sigma_d}^c(t_l) = \left[\sigma_d + \frac{P_p\lambda_p}{\lambda_p - \lambda_d}\sigma_p\right] - \frac{P_p\lambda_d\sigma_p\exp((\lambda_d - \lambda_p)t_l)}{\lambda_p - \lambda_d}\frac{[1 - \exp(-\lambda_p t_i)]}{[1 - \exp(-\lambda_d t_i)]}. \tag{A10}$$

This equation connects the cumulative and the independent cross section of the daughter and the cross section of the parent.

[1] R. A. Broglia and A. Winther, *Heavy Ion Reactions: Elastic and Inelastic Reactions*, Vol. 1 (Benjamin-Cummings Publishing Company, Reading, MA, 1981).
[2] K. Rehm, Annu. Rev. Nucl. Part. Sci. **41**, 429 (1991).
[3] P. Woods and C. Davids, Annu. Rev. Nucl. Part. Sci. **47**, 541 (1997).
[4] W. Von Oertzen and A. Vitturi, Rep. Prog. Phys. **64**, 1247 (2001).
[5] L. Corradi, G. Pollarolo, and S. Szilner, J. Phys. G: Nucl. Part. Phys. **36**, 113101 (2009).
[6] B. B. Back, H. Esbensen, C. L. Jiang, and K. E. Rehm, Rev. Mod. Phys. **86**, 317 (2014).
[7] A. Denikin, A. Karpov, and N. Rowley, *Lecture Notes in Physics*, Vol. 963 (Springer Verlag, Berlin, 2019).
[8] H. Lenske, F. Cappuzzello, M. Cavallaro, and M. Colonna, Prog. Part. Nucl. Phys. **109**, 103716 (2019).
[9] C. Jiang, B. Back, K. Rehm, K. Hagino, G. Montagnoli, and A. Stefanini, European Phys. J. A **57**, 1 (2021).
[10] A. Zucker, Annu. Rev. Nucl. Sci. **10**, 27 (1960).
[11] H. Doubre, Europhysics News **15**, 10 (1984).
[12] M. A. Stoyer, Nature (London) **442**, 876 (2006).
[13] L. R. Gasques, A. V. Afanasjev, E. F. Aguilera, M. Beard, L. C. Chamon, P. Ring, M. Wiescher, and D. G. Yakovlev, Phys. Rev. C **72**, 025806 (2005).

[14] L. R. Gasques, E. F. Brown, A. Chieffi, C. L. Jiang, M. Limongi, C. Rolfs, M. Wiescher, and D. G. Yakovlev, Phys. Rev. C **76**, 035802 (2007).
[15] C. Ngô, Prog. Part. Nucl. Phys. **16**, 139 (1986).
[16] J. V. Kartz, J. O. Liljenzin, A. E. Norris, and G. T. Seaborg, Phys. Rev. C **13**, 2347 (1976).
[17] G. K. Gubbi, A. Goswami, B. S. Tomar, A. Ramaswami, A. V. R. Reddy, P. P. Burte, S. B. Manohar, and B. John, Phys. Rev. C **59**, 3224 (1999).
[18] D. J. Hinde *et al.*, J. Phys.: Conf. Ser. **420**, 012115 (2013).
[19] W. Gawlikowicz, D. K. Agnihotri, S. A. Baldwin, W. U. Schröder, J. Töke, R. J. Charity, D. G. Sarantites, L. G. Sobotka, R. T. deSouza, T. Barczyk, K. Grotowski, S. Micek, R. Płaneta, and Z. Sosin, Phys. Rev. C **81**, 014604 (2010).
[20] L. W. Alvarez, Phys. Rev. **52**, 134 (1937).
[21] C. D. Anderson, Nature (London) **133**, 313 (1934).
[22] M. Cavinato, E. Fabrici, E. Gadioli, E. Gadioli Erba, P. Vergani, M. Crippa, G. Colombo, I. Redaelli, and M. Ripamonti, Phys. Rev. C **52**, 2577 (1995).
[23] A. Yadav, V. R. Sharma, P. P. Singh, D. P. Singh, M. K. Sharma, U. Gupta, R. Kumar, B. P. Singh, R. Prasad, and R. K. Bhowmik, Phys. Rev. C **85**, 034614 (2012).
[24] A. Yadav, P. P. Singh, M. Shuaib, V. R. Sharma, I. Bala, Unnati, S. Gupta, D. P. Singh, M. K. Sharma, R. Kumar, S. Murlithar, R. P. Singh, B. P. Singh, and R. Prasad, Phys. Rev. C **96**, 044614 (2017).
[25] P. K. Giri, A. Mahato, D. Singh, S. B. Linda, H. Kumar, S. A. Tali, M. A. Ansari, R. Kumar, S. Muralithar, and R. P. Singh, Phys. Rev. C **100**, 054604 (2019).
[26] A. Mahato *et al.*, Eur. Phys. J. A **56**, 131 (2020).
[27] R. Prasad and B. P. Singh, Experimental details and formulations, in *Fundamentals and Applications of Heavy Ion Collisions: Below 10 MeV/ Nucleon Energies* (Cambridge University Press, Cambridge, 2018), pp. 88–130.
[28] J. F. Ziegler *et al.*, Nucl. Instrum. Methods Phys. Res. B **268**, 1818 (2010), 19th International Conference on Ion Beam Analysis.
[29] E. T. Subramaniam *et al.*, Rev. Sci. Instrum. **77**, 096102 (2006).
[30] K. Krane and D. Halliday, *Introductory Nuclear Physics* (Wiley, New York, 1987).
[31] B. R. Martin, *Nuclear and Particle Physics* (Wiley, New York, 2006).
[32] E. V. Sayre, Annu. Rev. Nucl. Sci. **13**, 145 (1963).
[33] G. Gyürky *et al.*, Eur. Phys. J. A **55**, 41 (2019).
[34] W. Rubinson, J. Chem. Phys. **17**, 542 (1949).
[35] J. Cetnar, Ann. Nucl. Energy **33**, 640 (2006).
[36] R. B. Firestone *et al.*, *The 8th Edition of the Table of Isotopes* (Springer, Hungary, 1997).
[37] A. Gavron, Phys. Rev. C **21**, 230 (1980).
[38] W. Hauser and H. Feshbach, Phys. Rev. **87**, 366 (1952).
[39] C. Perey and F. Perey, At. Data Nucl. Data Tables **17**, 1 (1976).
[40] R. Bass, Phys. Rev. Lett. **39**, 265 (1977).
[41] S. K. Kataria, V. S. Ramamurthy, and S. S. Kapoor, Phys. Rev. C **18**, 549 (1978).
[42] A. Gilbert and A. Cameron, Can. J. Phys. **43**, 1446 (1965).